Solvent vapor annealing of block copolymers in confined topographies: commensurability considerations for nanolithography

Cian Cummins,* Roisin A. Kelly, Anushka Gangnaik, Yordan M. Georgiev, Nikolay Petkov, Justin D. Holmes and Michael A. Morris*

C. Cummins, Prof. M.A. Morris
Materials Research Group, Department of Chemistry and Tyndall National Institute, University College Cork, Cork, Ireland.
Centre for Research on Adaptive Nanostructures and Nanodevices (CRANN/AMBER), Trinity College Dublin, Dublin, Ireland.
*Corresponding Authors: m.morris@ucc.ie, cian.a.cummins@gmail.com

R.A. Kelly, A. Gangnaik, Prof. Y.M. Georgiev, N. Petkov, Prof. J.D. Holmes
Materials Chemistry and Analysis Group, Department of Chemistry and Tyndall National Institute, University College Cork, Cork, Ireland.
Centre for Research on Adaptive Nanostructures and Nanodevices (CRANN/AMBER), Trinity College Dublin, Dublin, Ireland.

Abstract

The directed self-assembly (DSA) of block copolymer (BCP) materials in topographically patterned substrates (*i.e.* graphoepitaxy) is a potential methodology for the continued scaling of nanoelectronic device technologies. In this communication, we report an unusual feature size variation in BCP nanodomains under confinement with graphoepitaxially aligned cylinder-forming poly(styrene)-*block*-poly(4-vinylpyridine) (PS-*b*-P4VP) BCP. Graphoepitaxy of PS-*b*-P4VP BCP line patterns (C_{II}) was accomplished via topography in hydrogen silsequioxane (HSQ) modified substrates and solvent vapor annealing (SVA). Interestingly, reduced domain sizes in features close to the HSQ guiding features were observed. The feature size reduction was evident after inclusion of alumina into the P4VP domains followed by pattern transfer to the substrate. We suggest that this nanodomain size perturbation is due to solvent swelling effects during SVA. We propose that using a commensurability value close to the solvent vapor annealed periodicity will alleviate this issue leading to uniform nanofins.

1. Introduction

Microphase separation of di-block copolymers (di-BCPs) can form sub-20 nm arrays of spherical, cylindrical, gyroidal and lamellar geometries that have potential in electronic, environmental and energy application.[1,2,3,4] In particular, BCP materials are of significant interest to chip manufacturers for use as on-chip etch masks for patterning future nanoelectronic circuitry.[5],[6] In order to align (to a substrate direction) the randomly oriented domain structures that result from microphase separation and, thus, allow the formation of the periodic arrangements needed for development of advanced device technologies such as Fin-type field-effect transistors (FinFETs),[7] directed self-assembly (DSA) is required. DSA is an absolute pre-requisite to attain the low defect density and overlay accuracy required for industrial integration.[8]

BCP self-assembly can be directed via pre-patterned chemical patterns (chemoepitaxy)[9,10] or using topographical patterns (graphoepitaxy).[11,12] Graphoepitaxy has been exploited in many BCP systems such as PS-*b*-PMMA (PS-*b*-polymethyl methacrylate),[13,14] PS-*b*-PDMS (PS-*b*-polydimethylsiloxane)[15,16] and PS-*b*-PVP.[17,18] DSA of BCP thin films through both thermal annealing[19] and solvent vapor annealing[20] (SVA) has been studied extensively and attention is being given to the selective removal of block components [21,22] or the inclusion of etch contrast agents to facilitate pattern transfer.[23]

Pattern transfer of BCP etch masks is probably the least studied aspect of published nanolithography work but is paramount for obtaining uniform integrated circuit elements. [24,25] This is particularly true for BCP materials with a high Flory-Huggins interaction parameter (χ) such as the PS-*b*-PVP systems (χ = 0.18 for PS-*b*-P2VP) since they can display low domain sizes.[26,27] This communication reports an important observation for graphoepitaxially aligned line space features of PS-*b*-P4VP (24 kg mol^{-1} – 9.5 kg mol^{-1}) BCP system which suggests that SVA of graphoepitaxially aligned patterns may be more complex than often considered.

2. Experimental

Solvents

Acetone (ACS reagent, ≥99.5%) chloroform (for HPLC, ≥99.9%, contains 0.5-1.0% ethanol as stabilizer), iso-propyl alcohol (LC-MS CHROMASOLV), ethanol (dehydrated, 200 proof), Tetrahydrofuran (inhibitor-free, CHROMASOLV Plus, for HPLC, ≥99.9%), Toluene

(CHROMASOLV, for HPLC, 99.9%), were purchased from Sigma-Aldrich and used without further purification. De-ionized water was used wherever necessary.

General Methods

Hydrogen silsequioxane (HSQ) substrate preparation

Ten × 10 mm bulk silicon ⟨100⟩ oriented substrates (nominal resistivity 0.001 Ω cm) were employed and were first patterned using a HSQ Electron Beam Lithography (Raith e-LiNE plus) process. The substrates were initially degreased via ultrasonication in acetone and iso-propanol (IPA) solutions (2 × 2 min), dried in flowing nitrogen gas and baked for 2 minutes at 393 K in an ambient atmosphere to remove any residual IPA. The substrates were then spin coated with a 2.4 wt % solution of HSQ (XR-1541 Dow Corning Corp.) in MIBK (methylisobutyl ketone) to produce a ~50 nm film of HSQ. The wafer was subsequently baked at 393 K in an ambient atmosphere for 3 minutes prior to transfer to the EBL system for exposure. Arrays of 50 nm wide lines at pitches of 32n nm were exposed, where n is an integer and $0 < n < 8$. Following electron beam exposure the samples were developed in an aqueous solution of 0.25 M NaOH, 0.7 M NaCl for 15 seconds, followed by rinsing in flowing DI water for 60 seconds and 15 seconds rinse in IPA. A process flow is shown in the supporting information (SI) for HSQ fabrication. The samples were then blown dry in flowing nitrogen gas. HSQ gratings were fabricated at pitches of 64, 96, 128, 160, 192, 224 and 265 nm (*i.e.* n = 2, 3, 4, 5, 6, 7 and 8). The HSQ dimensions, PS-*b*-P4VP and alumina feature size, domain sizes *etc.* were measured through analysis of SEM and TEM images using ImageJ software. Note that the 265 nm (n = 8.28) HSQ grating value was higher than the expected 256 nm (n = 8) and this variation can be attributed to a higher exposure dose. Larger HSQ pitches were also fabricated at 285 nm and 350 nm as detailed below.

PS-*b*-P4VP BCP thin film deposition, solvent vapor annealing and film 'activation'

Poly(styrene)-*block*-poly(4-vinylpyridine) was purchased from Polymer Source, Inc., Canada, with a molecular weight of M_n = 33.5 kg mol^{-1} (M_{nPS} = 24 kg mol^{-1}; M_{nP4VP} = 9.5 kg mol^{-1}, f_{PS} = 0.70), a polydispersity (M_w/M_n) of 1.15 (where, M_n and M_w are number average and weight average molecular weights) and was used as received. Solutions of 0.5 weight % PS-*b*-P4VP BCP were prepared in toluene/THF (80:20). The solutions were left stirring for 12 hours to ensure complete dissolution. Prior to spin coating planar Si or HSQ substrates were sonicated for 20 minutes with acetone. The substrates were then rinsed in acetone and blown dry with nitrogen. Spin coating of the PS-*b*-P4VP solution was carried out at 3200 rpm for 30 seconds. Solvent vapor annealing was carried out in the conventional manner with a small vial containing 8–10 ml of chloroform placed inside a glass jar (150 ml) with PS-*b*-P4VP sample

for ~ 2 hours (room temperature ~ 290 K). After removing samples and leaving excess solvent to evaporate, the solvent vapor annealed films (with a thickness of 25 nm) were further exposed to ethanol vapors for surface reconstruction. In order to create a nanoporous PS-*b*-P4VP film for metal-salt inclusion, films were exposed to ethanol vapors for 'activation'. Conventional solvent vapor annealing was carried out by placing the self-assembled PS-*b*-P4VP film in a jar containing a vial with ~8 ml of ethanol solvent. Films were exposed to the ethanol vapors for 15-20 minutes. The films were then removed and left to dry/deswell at room temperature (~ 290 K). The resulting nanoporous line pattern was subsequently spin coated with the aluminium nitrate ethanol solution described below.

Metal oxide (alumina) nanowire fabrication

$Al(NO_3)_3.9H_2O$ (aluminium nitrate nonahydrate, ACS reagent, ≥98%) was employed as the metal nitrate salt precursor for inclusion to act as a hardmask (etchstop). Solutions of 0.4 wt % $Al(NO_3)_3.9H_2O$ were prepared in ethanol and spin-coated on to the ethanol reconstructed samples at 3200 rpm for 30 seconds. UV/O_3 treatment was used to oxidize the precursor and remove polymer. Samples were UV/O_3 treated in a UV/ozone system (PSD Pro Series Digital UV Ozone System; Novascan Technologies, Inc., USA).

Pattern Transfer Etch Procedure

An STS, Advanced Oxide Etch (AOE) ICP etcher was used to pattern transfer alumina nanowires to the underlying Si substrate. Nanofin fabrication was carried out by using a controlled gas mixture of C_4F_8/SF_6 at flow rates of 90 sccm/30 sccm and the ICP and RIE power were set to 600 W and 15 W respectively at a chamber pressure of 15 mTorr. Alumina nanowires were etched using C_4F_8/SF_6 Si etch recipe. Nanofins shown in Figure 1c,d, Figure 2 and Figure 3 result from a Si etch of 1 minute and 30 seconds. Nanofins shown in Figure 4 were fabricated after using the Si etch for 2 minutes. Note that most of the original HSQ material has been consumed during the etching process and is indicated in TEM images to show initial placement for the reader.

Instrumentation and Characterization

Block copolymer film thicknesses were measured with a spectroscopic ellipsometer "J.A. Woollam Ellipsometer" at a fixed angle of incidence of 70°, on at least three different places on the sample and was averaged as the film thickness. A two layer model (SiO_2 + PS-*b*-P4VP) for total BCP film was used to simulate experimental data. Scanning Electron Microscopy (SEM) images were obtained by a FEI Helios Nanolab 600i system at an accelerating voltage of 5 kV and at a working distance of 4 mm. Transmission Electron Microscopy (TEM) lamella specimen were prepared using the Helios NanoLab DB FIB. FIB samples were analysed by

JEOL 2100 high resolution transmission electron microscope operating at an accelerating voltage of 200 kV.

3. Results and Discussion

Scheme 1 outlines the process for fabricating Si nanofins directed in HSQ trenches. Self-assembly of PS-*b*-P4VP BCP thin films was induced via SVA in a chloroform atmosphere at room temperature (~ 290 K). P4VP cylinders were orientated parallel (C_{II}) to the substrate, forming 'fingerprint' patterns with a 32 nm periodicity. P4VP cylinder dimensions were measured at 20 nm. These patterns were guided and aligned in HSQ trenches of varying pitch (the nominal HSQ pitch was 32n nm where n is an integer and $0 < n < 8$). An ethanol vapor treatment was employed to 'activate' the PS-*b*-P4VP thin film creating a nanoporous structure.[28,29] This process introduces free volume to assist the salt inclusion process.[30,31] The selective inclusion of the salt into the P4VP block of the 'activated' nanoporous films was achieved via spin coating of an ethanolic solution of aluminium nitrate. Following deposition of the metal-salt ethanolic precursor, ultraviolet/ozone exposure was carried out for 3 hours leading to the formation of γ-Al_2O_3 (alumina) nanowires at the substrate surface.

Figure 1a shows uniform alumina nanowires after metal-oxide inclusion on an open area of the patterned HSQ substrate. Figure 1b displays a top-down SEM image of alumina nanowires graphoepitaxially aligned within ~ 50 nm HSQ gratings at a pitch of ~ 265 nm. Seven alumina nanowire features mimicking the original P4VP structure can be seen. Si nanofins resulting from pattern transfer of the alumina nanowire hardmask from an open area of the HSQ patterned substrate are shown in figure 1c. Figure 1d shows a top-down SEM image corresponding to Si nanofins fabricated from pattern transfer of DSA graphoepitaxy features. Etch recipes for pattern transfer are detailed in the experimental section. It is clear from Figure 1d that the nanofins closest to the sidewall are considerably smaller in feature size than the five nanofins in the centre of the channel (feature sizes of 6 and 12 nm respectively). The occurrence of this reduction in feature sizes was observed in several areas of HSQ arrays (10 x 10 micron each) and across varying HSQ periodicities (>100 nm). Figure 2 displays top-down SEM images of Si nanofins in 128 nm and 224 nm pitch HSQ gratings where sidewall nanofin feature size reduction is evident. As mentioned, this is in contrast to the uniform nanofins made on planar substrate areas, as there is no variation in feature size (figure 1c). Also, there was no variation in feature size observed with Si etch time. Corresponding TEM data of the Si nanofins from the ~ 265 nm arrays (Figure 1d) are displayed in Figure 3 following pattern transfer to the

substrate and it is clear that the alumina nanowires closest to the HSQ sidewalls have produced deeper Si nanofins (up to ~ 15 nm) than the nanofins at the centre of the channel, which is consistent with enhanced etching in the more confined space.

To further show that this feature size variation was not a direct result of either the etch procedure or geometry related etch effects, we show data for pattern transfer of the BCP metal oxide enhanced structures formed in channels of ~ 285 nm and ~ 350 nm respectively (Figures 4a and 4b). These widths are too large for good DSA and a non-aligned arrangement is observed. An indicative TEM image is displayed in figure 4c of Si nanofins fabricated via pattern transfer (350 nm channels) in confinement of aligned patterns only.

To explain the observations we suggest that the solvent swelling that occurs during SVA is the cause of these complex structures. The dimensions of the channels were set according to the dimensions of the pattern seen on planar surfaces after solvent induced microphase separation. This is explained in Scheme 1A and is set at number of domain spacings (DS) plus 2(r+s) where r = cylinder radius and s = half cylinder edge to cylinder edge distance. Thus, the HSQ grating pitches employed were set at 32n (where 0 > n > 8) nm. Whilst this approach is established for thermally annealed systems where polymer expansion is limited, in SVA there is a considerable expansion due to solvent swelling and this results in both film expansion and non-ideal feature spacing (Scheme 1B). The expansion might result in curvature at the side walls in the plane of the cylinders to allow optimum cylinder separation and also due to sidewall-polymer interfacial interactions. We have shown previously that removal from the solvent atmosphere results in rapid film shrinkage and residual material at sidewalls as the solvent front moves rapidly through the film.[32] A direct result is a change in cylinder shape from a cylindrical to an elliptical cross-section.[33,34] The shape of the film in the channel results in a tilt of the cylinders close to the sidewall after the release of solvent following SVA (Scheme 1C). In certain instances, this might result in polymer being isolated at the top of the channel walls due to the additional binding at these edge sites. In Scheme 1D, ethanol is used to selectively swell the P4VP domains (see experimental for details) to create a nanoporous matrix assisting the metal-salt inclusion technique. In Scheme 1E the results of metal ion oxidation and polymer removal can be seen and in particular reduction of the alumina dimensions because of the smaller footprint (due to elliptical tilting and also partial volume reduction with material remaining at the edge of the mesa) of the P4VP derived feature. On pattern transfer (Scheme 1F), the narrow alumina features provide thinner Si features. Also because of the smaller dimensions, an enhanced etch rate (compared to the larger features) is observed due to gas confinement and aspect-ratio dependent etching (ARDE). It is quite apparent that the

features are not only narrower but deeper into the substrate from TEM data (figure 3). The enhanced etching of Si material near the HSQ gratings in figure 3 may be a direct result of the wider dimensions of the HSQ itself (with respect to the alumina nanowires). Furthermore, ARDE and other plasma issues are visible at the larger alumina features as these have produced a smaller aspect ratio in comparison to the sidewall alumina features. One can see that the proximity of the larger alumina mask features has resulted in a slower etch. The non-uniformity of the resultant Si etch could be alleviated through process flows integrating sidewall passivation methods. Employing passivated Si etches (*e.g.* pulsed-mode or mixed mode) can improve anisotropy of the Si etch[35] while protecting sidewall features.

4. Conclusion

The work presented here has significant importance in the application of BCP methods for producing ultra-fine features at substrates requiring the use of polymers that can only be annealed by solvent treatment. In nanolithography, methods must be developed that not only produce translational periodicity but also precisely and reproducibly create features of uniform dimensions. This work suggests feature size variation may be more challenging than expected. In order to alleviate the issues observed we believe trenches that are larger than the ideal commensurability (domain periodicity) of the BCP may be needed to allow for extra swelling. The additional 'expansion' volume will be dependent on the degree of swelling which will be related to the solvent-polymer interactions, vapor pressure and temperature.

Supporting Information

Schematic for HSQ patterning on silicon substrates is displayed in SI. SEM images of a HSQ patterned substrate with 128 nm pitch is also shown in SI.

Notes

The authors declare no competing financial interest.

Acknowledgments

The authors gratefully acknowledge Science Foundation Ireland (SFI) (Grant Number 09/IN.1/602) CSET/CRANN for funding this project. The authors also thank Alan Hydes for etching assistance.

Keywords: Block Copolymers, Directed Self-Assembly, Solvent Vapor Annealing, Commensurability, Graphoepitaxy, Pattern Transfer.

1. Farrell, R. A.; Petkov, N.; Morris, M. A.; Holmes, J. D., Self-assembled templates for the generation of arrays of 1-dimensional nanostructures: From molecules to devices. *Journal of Colloid and Interface Science* **2010,** *349* (2), 449-472.
2. Bang, J.; Jeong, U.; Ryu, D. Y.; Russell, T. P.; J Hawker, C., Block copolymer nanolithography: Translation of molecular level control to nanoscale patterns. *Advanced Materials* **2009,** *21* (47), 4769-4792.
3. Hillmyer, M., Nanoporous Materials from Block Copolymer Precursors. In *Block Copolymers II*, Abetz, V., Ed. Springer Berlin Heidelberg: 2005; Vol. 190, pp 137-181.
4. Topham, P. D.; Parnell, A. J.; Hiorns, R. C., Block copolymer strategies for solar cell technology. *Journal of Polymer Science Part B: Polymer Physics* **2011,** *49* (16), 1131-1156.
5. Morris, M. A., Directed self-assembly of block copolymers for nanocircuitry fabrication. *Microelectronic Engineering* **2014**.
6. Gay, G.; Baron, T.; Agraffeil, C.; Salhi, B.; Chevolleau, T.; Cunge, G.; Grampeix, H.; Tortai, J. H.; Martin, F.; Jalaguier, E.; Salvo, B. D., CMOS compatible strategy based on selective atomic layer deposition of a hard mask for transferring block copolymer lithography patterns. *Nanotechnology* **2010,** *21* (43), 435301.
7. Jeong, S.-J.; Kim, J. Y.; Kim, B. H.; Moon, H.-S.; Kim, S. O., Directed self-assembly of block copolymers for next generation nanolithography. *Materials Today* **2013,** *16* (12), 468-476.
8. Doerk, G. S.; Liu, C.-C.; Cheng, J. Y.; Rettner, C. T.; Pitera, J. W.; Krupp, L. E.; Topuria, T.; Arellano, N.; Sanders, D. P., Pattern Placement Accuracy in Block Copolymer Directed Self-Assembly Based on Chemical Epitaxy. *ACS Nano* **2012,** *7* (1), 276-285.
9. Stoykovich, M. P.; Kang, H.; Daoulas, K. C.; Liu, G.; Liu, C.-C.; de Pablo, J. J.; Müller, M.; Nealey, P. F., Directed Self-Assembly of Block Copolymers for Nanolithography: Fabrication of Isolated Features and Essential Integrated Circuit Geometries. *ACS Nano* **2007,** *1* (3), 168-175.
10. Delgadillo, P. A. R.; Gronheid, R.; Thode, C. J.; Wu, H.; Cao, Y.; Neisser, M.; Somervell, M.; Nafus, K.; Nealey, P. F., Implementation of a chemo-epitaxy flow for directed self-assembly on 300-mm wafer processing equipment. *MOEMS* **2012,** *11* (3), 031302-1-031302-5.
11. Hobbs, R. G.; Petkov, N.; Holmes, J. D., Semiconductor nanowire fabrication by bottom-up and top-down paradigms. *Chemistry of Materials* **2012,** *24* (11), 1975-1991.
12. Bita, I.; Yang, J. K. W.; Jung, Y. S.; Ross, C. A.; Thomas, E. L.; Berggren, K. K., Graphoepitaxy of Self-Assembled Block Copolymers on Two-Dimensional Periodic Patterned Templates. *Science* **2008,** *321* (5891), 939-943.
13. Tsai, H.; Pitera, J. W.; Miyazoe, H.; Bangsaruntip, S.; Engelmann, S. U.; Liu, C.-C.; Cheng, J. Y.; Bucchignano, J. J.; Klaus, D. P.; Joseph, E. A.; Sanders, D. P.; Colburn, M. E.; Guillorn, M. A., Two-Dimensional Pattern Formation Using Graphoepitaxy of PS-*b*-PMMA Block Copolymers for Advanced FinFET Device and Circuit Fabrication. *ACS Nano* **2014,** *8* (5), 5227-5232.
14. Borah, D.; Rassapa, S.; Shaw, M. T.; Hobbs, R. G.; Petkov, N.; Schmidt, M.; Holmes, J. D.; Morris, M. A., Directed self-assembly of PS-*b*-PMMA block copolymer using HSQ lines for translational alignment. *Journal of Materials Chemistry C* **2013,** *1* (6), 1192-1196.

15. Borah, D.; Rasappa, S.; Senthamaraikannan, R.; Holmes, J. D.; Morris, M. A., Graphoepitaxial Directed Self-Assembly of Polystyrene-*Block*-Polydimethylsiloxane Block Copolymer on Substrates Functionalized with Hexamethyldisilazane to Fabricate Nanoscale Silicon Patterns. *Advanced Materials Interfaces* **2014,** *1* (3).
16. Hobbs, R. G.; Farrell, R. A.; Bolger, C. T.; Kelly, R. A.; Morris, M. A.; Petkov, N.; Holmes, J. D., Selective Sidewall Wetting of Polymer Blocks in Hydrogen Silsesquioxane Directed Self-Assembly of PS-*b*-PDMS. *ACS Applied Materials & Interfaces* **2012,** *4* (9), 4637-4642.
17. Chai, J.; Wang, D.; Fan, X.; Buriak, J. M., Assembly of aligned linear metallic patterns on silicon. *Nature Nanotechnology* **2007,** *2* (8), 500-506.
18. Park, S.; Kim, B.; Yavuzcetin, O.; Tuominen, M. T.; Russell, T. P., Ordering of PS-*b*-P4VP on Patterned Silicon Surfaces. *ACS Nano* **2008,** *2* (7), 1363-1370.
19. Bates, C. M.; Maher, M. J.; Janes, D. W.; Ellison, C. J.; Willson, C. G., Block Copolymer Lithography. *Macromolecules* **2013,** *47* (1), 2-12.
20. Sinturel, C.; Vayer, M.; Morris, M.; Hillmyer, M. A., Solvent Vapor Annealing of Block Polymer Thin Films. *Macromolecules* **2013,** *46* (14), 5399-5415.
21. Cummins, C.; Mokarian-Tabari, P.; Holmes, J. D.; Morris, M. A., Selective etching of polylactic acid in poly(styrene)-*block*-poly(d,l)lactide diblock copolymer for nanoscale patterning. *Journal of Applied Polymer Science* **2014,** *131* (18).
22. Olayo-Valles, R.; Lund, M. S.; Leighton, C.; Hillmyer, M. A., Large area nanolithographic templates by selective etching of chemically stained block copolymer thin films. *Journal of Materials Chemistry* **2004,** *14* (18), 2729-2731.
23. Cummins, C.; Borah, D.; Rasappa, S.; Chaudhari, A.; Ghoshal, T.; O'Driscoll, B. M. D.; Carolan, P.; Petkov, N.; Holmes, J. D.; Morris, M. A., Self-assembly of polystyrene-*block*-poly(4-vinylpyridine) block copolymer on molecularly functionalized silicon substrates: fabrication of inorganic nanostructured etchmask for lithographic use. *Journal of Materials Chemistry C* **2013,** *1* (47), 7941-7951.
24. Gu, X.; Gunkel, I.; Russell, T. P., Pattern transfer using block copolymers. *Philosophical Transactions of the Royal Society A: Mathematical, Physical and Engineering Sciences* **2013,** *371* (2000).
25. Borah, D.; Shaw, M. T.; Rasappa, S.; Farrell, R. A.; Mahony, C. O.; Faulkner, C. M.; Bosea, M.; Gleeson, P.; Holmes, J. D.; Morris, M. A., Plasma etch technologies for the development of ultra-small feature size transistor devices. *Journal of Physics D: Applied Physics* **2011,** *44* (17), 174012.
26. Gu, X.; Liu, Z.; Gunkel, I.; Chourou, S. T.; Hong, S. W.; Olynick, D. L.; Russell, T. P., High Aspect Ratio Sub-15 nm Silicon Trenches From Block Copolymer Templates. *Advanced Materials* **2012,** *24* (42), 5688-5694.
27. Gu, X.; Dorsey, P.; Russell, T. P., High density and large area arrays of silicon oxide pillars with tunable domain size for mask etch applications. *Advanced Materials* **2012,** *24* (40), 5505-5511.
28. Bhoje Gowd, E.; Nandan, B.; Vyas, M. K.; Bigall, N. C.; Eychmüller, A.; Schlörb, H.; Stamm, M., Highly ordered palladium nanodots and nanowires from switchable block copolymer thin films. *Nanotechnology* **2009,** *20* (41).
29. Ghoshal, T.; Senthamaraikannan, R.; Shaw, M. T.; Holmes, J. D.; Morris, M. A., Fabrication of Ordered, Large Scale, Horizontally-Aligned Si Nanowire Arrays Based on an In Situ Hard Mask Block Copolymer Approach. *Advanced Materials* **2013**.
30. Kim, S. H.; Misner, M. J.; Yang, L.; Gang, O.; Ocko, B. M.; Russell, T. P., Salt complexation in block copolymer thin films. *Macromolecules* **2006,** *39* (24), 8473-8479.

31. Ghoshal, T.; Shaw, M. T.; Bolger, C. T.; Holmes, J. D.; Morris, M. A., A general method for controlled nanopatterning of oxide dots: a microphase separated block copolymer platform. *Journal of Materials Chemistry* **2012,** *22* (24), 12083-12089.
32. Fitzgerald, T. G.; Farrell, R. A.; Petkov, N.; Bolger, C. T.; Shaw, M. T.; Charpin, J. P. F.; Gleeson, J. P.; Holmes, J. D.; Morris, M. A., Study on the Combined Effects of Solvent Evaporation and Polymer Flow upon Block Copolymer Self-Assembly and Alignment on Topographic Patterns. *Langmuir* **2009,** *25* (23), 13551-13560.
33. Borah, D.; Shaw, M. T.; Holmes, J. D.; Morris, M. A., Sub-10 nm Feature Size PS-*b*-PDMS Block Copolymer Structures Fabricated by a Microwave-Assisted Solvothermal Process. *ACS Applied Materials & Interfaces* **2013,** *5* (6), 2004-2012.
34. O'Driscoll, B. M. D.; Kelly, R. A.; Shaw, M.; Mokarian-Tabari, P.; Liontos, G.; Ntetsikas, K.; Avgeropoulos, A.; Petkov, N.; Morris, M. A., Achieving structural control with thin polystyrene-*b*-polydimethylsiloxane block copolymer films: The complex relationship of interface chemistry, annealing methodology and process conditions. *European Polymer Journal* **2013,** *49* (11), 3445-3454.
35. Henry, M. D., ICP Etching of Silicon for Micro and Nanoscale Devices. *PhD Thesis* **2010,** *California Institute of Technology*.

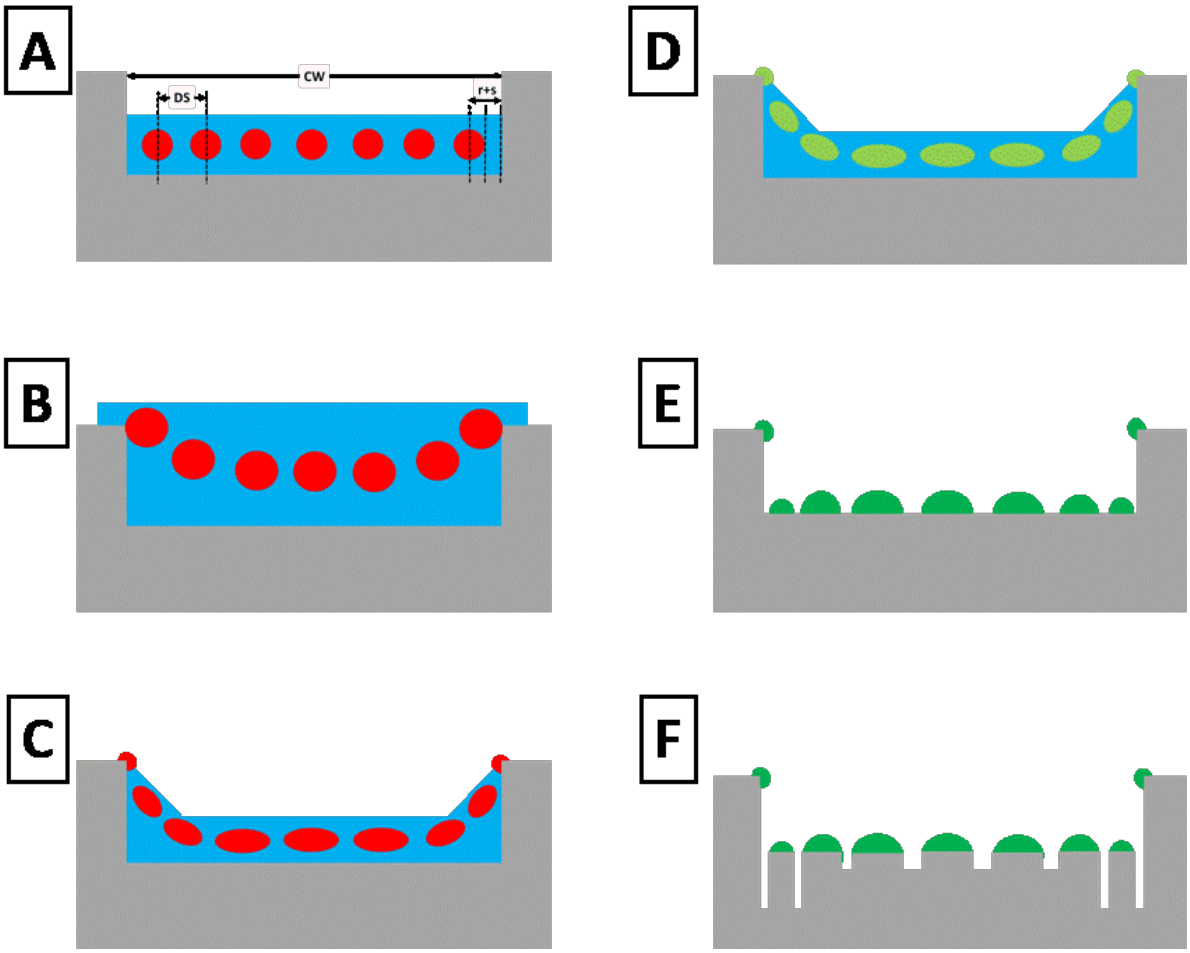

Scheme 1. Outline of the swelling phenomenon occurring during solvent vapor annealing of PS-*b*-P4VP BCP graphoepitaxially aligned by HSQ gratings and fabrication of Si nanofins from side-view perspective. (a) Spin coated PS-*b*-P4VP film, note that ordered equilibrium structures are shown for simplicity. BCP film shows majority PS (blue) matrix and minority P4VP cylinders (red). (b) Swelling of film and expansion when exposed to chloroform during solvent vapor annealing. (c) Film after release of solvent vapor. (d) Exposure to ethanol vapor for 20 minutes during 'activation' step to create nanoporous structure, swollen P4VP domains (light green). (e) Fabrication of alumina (dark green) nanowires after spin coating of aluminium nitrate ethanol precursor on nanoporous PS-*b*-P4VP film followed by UV/O_3. (f) Pattern transfer of alumina nanowire hardmask (etchstop) using dry etch procedure to underlying Si.

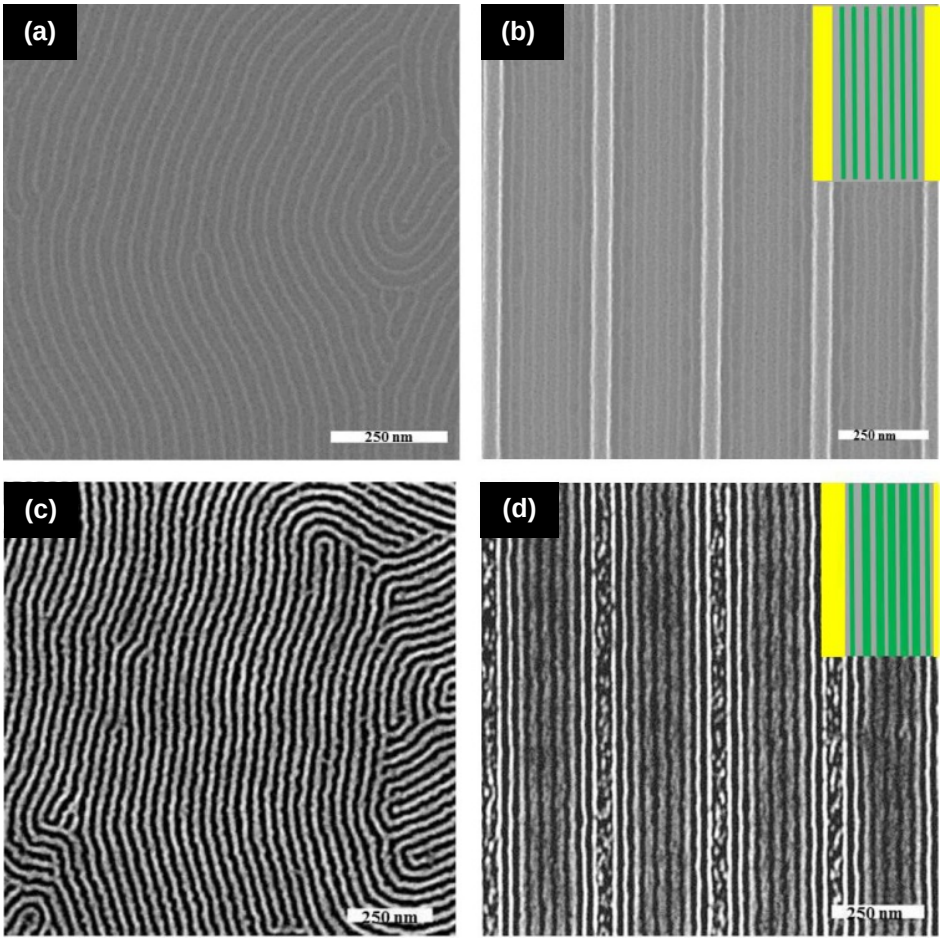

Figure 1. Top-down SEM image of (a) large open area of alumina nanowires and (b) alignment of alumina nanowires within HSQ trenches of ~ 265 nm pitch. Green bars represent the alumina nanowires while yellow bars represent the guiding HSQ gratings, (c) open area of Si nanofins following plasma etching of the alumina nanowires on the HSQ patterned Si substrate surface and (d) area of aligned Si nanofins HSQ trenches of ~ 265 nm pitch. Note that green bars in (d) represent Si nanofins. It is evident that the nanofins closer to the sidewalls are smaller in diameter.

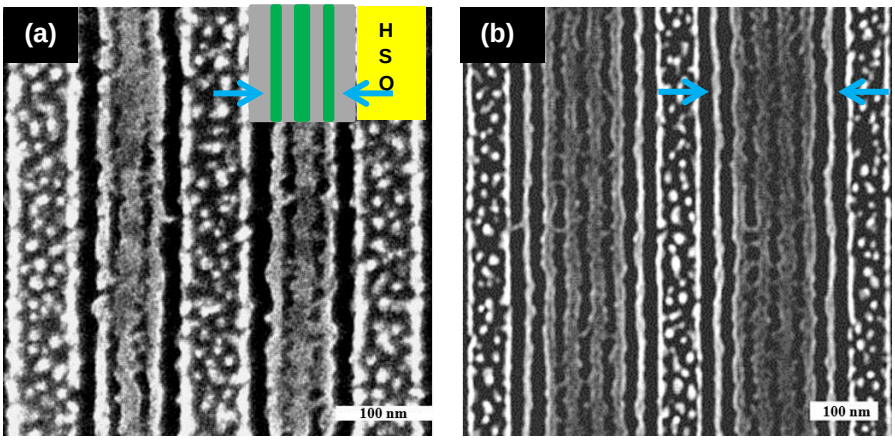

Figure 2. Top-down SEM image of (a) 3 Si nanofins within 128 nm HSQ gratings and (b) 6 Si nanofins within 224 nm HSQ gratings. Nanofins aligned next to the HSQ gratings show reduced feature sizes in comparison to the remaining Si nanofins. Green lines in (a) represent Si nanofins. Arrows in (a) and (b) point to the reduced feature sizes of nanofins next to HSQ gratings.

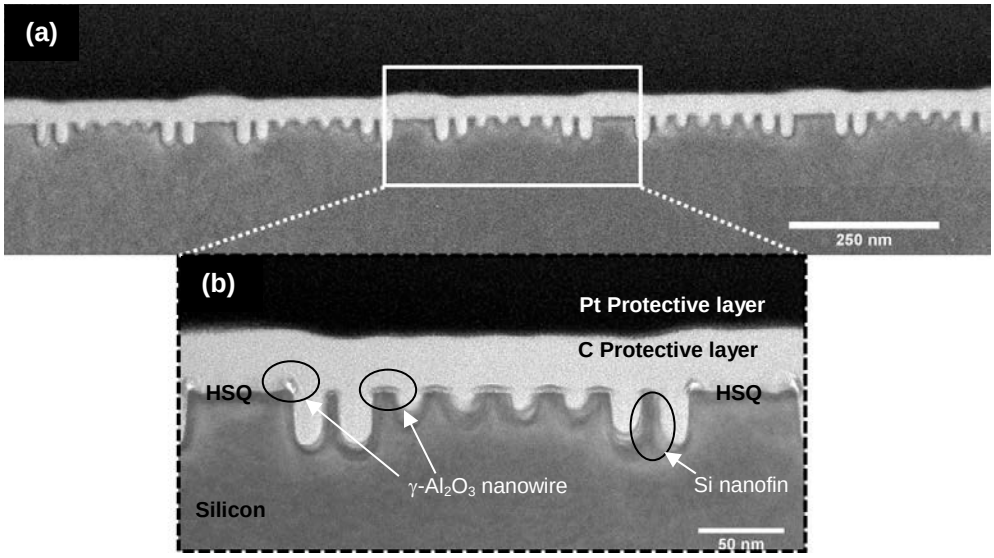

Figure 3. (a) Cross-section TEM image of large area of Si nanofins following pattern transfer of alumina nanowire hardmask in ~ 265 nm pitch HSQ trenches. (b) High resolution TEM image of Si nanofins between HSQ gratings where the reduced Si nanofin feature size and increased etch depth at the HSQ sidewalls is evident.

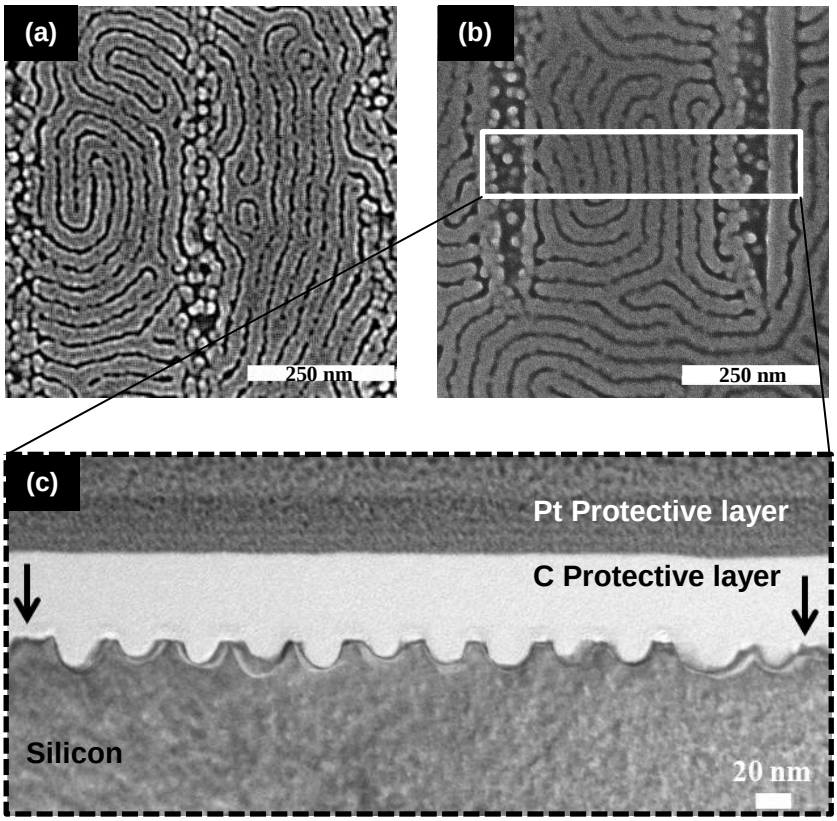

Figure 4. Top-down SEM images of Si nanofins in HSQ trenches of (a) ~ 285 nm and (b) ~ 350 nm respectively. (c) Cross-section TEM of Si nanofins fabricated from alumina nanowires acting as a hardmask in HSQ trenches. The pitch of the HSQ trenches was 350 nm. Arrows in (c) indicate where HSQ gratings were prior to etching. With a larger HSQ pitch and slightly increased commensurability compared to the ideal (32n), reduced features were not observed at the sidewalls.

For table of contents use only.